PCCP

RSC Publishing

PERSPECTIVE

View Article Online
View Journal

Cite this: DOI: 10.1039/c3cp51930a

Studies of bimolecular reaction dynamics using pulsed high-intensity vacuum-ultraviolet lasers for photoionization detection

Daniel R. Albert and H. Floyd Davis*

Received 7th May 2013,
Accepted 11th July 2013

DOI: 10.1039/c3cp51930a

www.rsc.org/pccp

This article describes recent progress on the development and application of pulsed high-intensity (~0.1 mJ per pulse) vacuum-ultraviolet (VUV) radiation produced by commercial tabletop lasers for studies of gas phase chemical reaction dynamics involving polyatomic free radicals. Our approach employs near-triply resonant four-wave mixing of *unfocussed* nanosecond dye lasers in an atomic gas as an alternative to the use of synchrotron light sources for sensitive universal soft photoionization detection of reaction products using a rotatable source crossed molecular beams apparatus with fixed detector. We illustrate this approach in studies of the reactions of phenyl radicals with molecular oxygen and with propene. Future prospects for the use of tabletop laser-based VUV sources for studies of chemical reaction dynamics are discussed.

1. Introduction

Crossed molecular beams experiments can provide extremely detailed insight into the dynamics of bimolecular elementary gas phase chemical reactions.[1–6] For three- or four-atom systems forming products that can be detected in a quantum state-resolved manner, experimentally-determined product angular, velocity and quantum state distributions can be compared to predictions derived from "exact" quantum scattering calculations.[7–9] For more complex polyatomic systems, the reaction dynamics may involve multiple mechanisms, often leading to more than one product channel. In such cases,[10] the identification of the primary product channels, measuring their branching ratios, and unraveling the microscopic reaction mechanisms, are usually the key goals of both experiment and theory.[11,12]

In studies of bimolecular reaction dynamics, the single-collision conditions offered by the crossed molecular beams method makes it possible to observe nascent products, frequently highly reactive radicals, without interference by secondary collisions. Unfortunately, the low reactant densities required to ensure single collision conditions makes product detection challenging.[2,4] The development of a crossed molecular beams apparatus[13] employing electron impact ionization followed by a quadrupole mass analyzer has facilitated studies of chemical systems ranging from simple 3-atom exchange reactions[14] to complex polyatomic reactions.[15] Electron impact mass spectrometry is a "universal" detection method, applicable to detection of any gaseous atom or molecule. Unfortunately, the sensitivity of electron impact detection is typically much lower than for methods based on electronic spectroscopy, such as laser induced fluorescence (LIF),[16,17] resonance-enhanced multi photon ionization (REMPI),[18–21] or Rydberg tagging time-of-flight (TOF) spectroscopy[22–25] However, LIF, REMPI and Rydberg tagging require detailed knowledge of the spectroscopic fingerprints of the species being detected. While the electronic spectroscopies of atoms and many diatomic molecules are well-characterized, the same can be said for only a relatively small number of triatomic (or larger) molecules. In addition, electronic excitation of polyatomic molecules may lead to photodissociation, thereby rendering LIF, REMPI and Rydberg tagging ineffective for detecting many molecular species.

In the field of bimolecular reaction dynamics involving free radicals, *atomic* free radicals have been studied most extensively, with the greatest focus on H, D, O, F, Cl, Br *etc.* Such species are readily produced in high yield and high purity by photolysis or pyrolysis of a stable precursor. Bimolecular reactions involving atomic free radicals usually proceed with large cross sections, often (but not always) forming a limited number of different products. On the other hand, *molecular* free radicals are more difficult to produce than atomic radicals, and often undergo self-reaction producing impurities. Furthermore, steric factors often play important roles in limiting reaction cross sections,[3] particularly for radicals containing 3

Department of Chemistry and Chemical Biology, Baker Laboratory, Cornell University, Ithaca, NY 14853-1301, USA. E-mail: hfd1@cornell.edu

or more atoms, and polyatomic free radical reactions often involve more than one channel. From these considerations, studies of polyatomic free radical reactions using crossed molecular beams are extremely challenging.

For several decades, "hard" electron impact ionization (using 60–100 eV electrons) was used in an effort to maximize ionization efficiencies (typically 0.01%).[2,4] However, interfering signals at the m/z ratio of interest often arise. Since the residual gases in a UHV chamber are primarily CO and H_2, detection at m/z = 28 and 2 is extremely difficult. To meet this challenge, Yang and coworkers employed extensive cryopumping and took special efforts to reduce pressures in the ionization region to $\sim 10^{-12}$ Torr, facilitating direct detection of even H_2 from photodissociation reactions.[26] However, there remains a less predictable source of background due to fragmentation of parent species producing unwanted daughter ions.[2] For example, methyl radicals (CH_3) can be produced by pyrolysis, photolysis, or electric discharge of molecular beams containing azomethane (CH_3NNCH_3). Although a significant fraction may be converted to CH_3, some undissociated azomethane will invariably be present and can undergo nonreactive collisions. Using hard electron impact ionization, fragmentation produces CH_3^+ (m/z = 15), N_2^+ (m/z = 28), N^+ (m/z = 14), $CH_3N_2^+$ (m/z = 43), CH_2^+ (m/z = 14), *etc.* Since background signals at these m/z ratios will be much larger than from bimolecular collisions of CH_3, detection of nonreactive scattering of CH_3 (m/z = 15), or reactions leading to production of C_2H_4 (m/z = 28), CH_2 (m/z = 14), or CH_3CO (m/z = 43) is likely to be impossible.[2]

As a direct consequence of the challenges associated with product detection in crossed beams experiments, the most readily-studied reactions are those producing molecules amenable to resonant detection methods such as REMPI or LIF. For reactions producing molecules not favorable to such detection methods, reactions with large cross sections and/or kinematics favorable for product detection have been studied most frequently. For example, the bimolecular reactions of phenyl radicals (C_6H_5) with propene (C_3H_6), of interest in connection with soot formation, involves addition of the radical to the C=C bond producing C_9H_{11}.[10,27–30] This reaction intermediate can decompose by loss of an H atom producing C_9H_{10}, or by CH_3 elimination producing C_8H_8.[28,30] The Newton diagrams in velocity space for these competing channels are shown in Fig. 1, with the circles denoting the maximum CM velocities of the C_9H_{10} and C_8H_8 products. Due to linear momentum conservation, the C_9H_{10} products are constrained to appear at a relatively narrow range of laboratory angles near the center of mass (CM) of the system, resulting in large product densities favorable to successful detection. The C_8H_8 products, on the other hand, recoil from the heavier CH_3 product and are scattered over a much larger range of angles. Assuming a 1 : 1 branching ratio and the same CM energy and angular distributions, the product signal intensities scale as the volume of the Newton sphere. In this case, the C_9H_{10} signal intensities at a given laboratory angle would be more than 50 times larger than signal intensities for the C_8H_8 channel, rendering it much easier to detect. The drawback, however, is that it is often difficult to extract much dynamical insight (CM angular and velocity distributions) by measuring the heavy products from H atom elimination, since their laboratory velocity distributions differ very little from that of the CM of the system.[31] More significant from a chemical perspective, many interesting reactions do not proceed exclusively by H atom elimination.

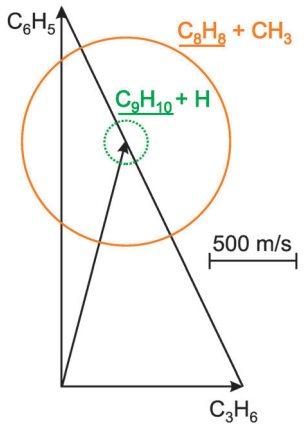

Fig. 1 Newton diagram in velocity space for the C_6H_5 + C_3H_6 reaction. The dotted circle corresponds to the maximum translational energy release of the C_9H_{10} + H product channel. The solid circle corresponds to the maximum translational energy release of the C_8H_8 + CH_3 product channel.

To overcome the limitations of dissociative ionization, Casavecchia and coworkers have elegantly demonstrated the use of low energy electrons for "soft" electron impact ionization detection of products from bimolecular reactions in crossed molecular beams.[11,15,32,33] By tuning the electron energies below that for dissociative ionization, interference from fragmentation of parent species may be reduced or eliminated. For example, since the ionization energy for CO (m/z = 28) is 14.0 eV, it is possible to detect species such as C_2H_4 (m/z = 28) with an ionization energy of 10.5 eV by tuning the electron energy around 11–13 eV. Unfortunately, this method comes with a substantial penalty; electron impact ionization cross sections decrease significantly at lower electron energies, leading to very small signal levels. Nevertheless, by decreasing the distances between nozzles and interaction region, Casavecchia and coworkers were able to compensate for the reduced ionization efficiencies and have mapped out the detailed dynamics for a wide variety of important chemical systems possessing multiple reaction pathways.[11,15,32,33]

Since the ionization energies of most molecules and free radicals exceed 8 eV (Fig. 2), there has been considerable interest in the use of "soft universal" photoionization detection using vacuum ultraviolet (VUV; λ < 180 nm) or extreme ultraviolet (XUV; λ < 110 nm) radiation.[34,35] The quasi-continuous VUV/XUV beam produced at third-generation synchrotrons such as Berkeley's Advanced Light Source[34] or Taiwan's Synchrotron Research Center[35] is broadly tunable in the 9–20 eV range, with $\sim$1% energy bandwidth, providing photon fluxes ($\sim 10^{16}$ photons per second[34,35]) that are sufficient for performing crossed molecular beam scattering experiments.[36–40] The primary limitation of this method is that third-generation synchrotron light sources are

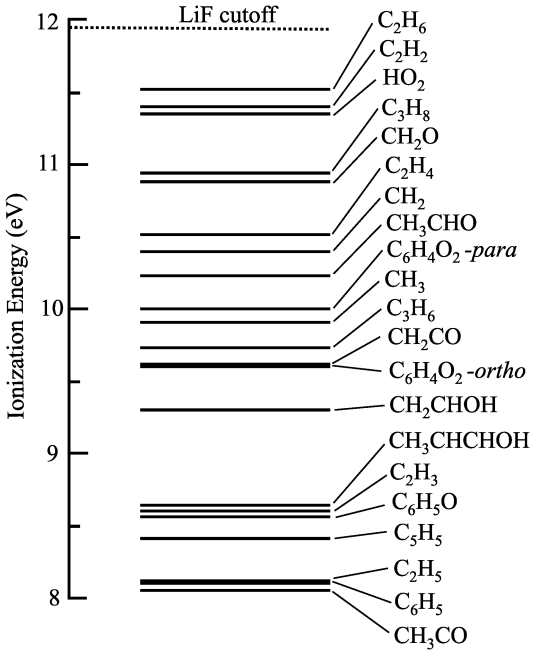

Fig. 2 Ionization energies of some simple molecules and radicals.

available at only a few locations worldwide. Also, due to the size and complexity of crossed molecular beams machines, successful implementation at a synchrotron requires a dedicated beamline for extended periods.

For studies of reactions of transition metal atoms with hydrocarbon molecules, the low ionization energies of metal-containing species has allowed the use of 7.9 eV photons from commercial F_2 excimer lasers (λ = 157 nm) for photoionization detection.[41–44] The performance of commercial 157 nm excimer lasers has improved greatly over the past couple of decades, and relatively inexpensive lasers producing >1 mJ per pulse at repetition rates of up to 100 Hz are readily available. The single photon ionization technique for transition metal atoms allowed for an increase of up to 100 in the signal to noise ratio, relative to electron impact ionization.[41] The improvement comes from both the increased detection efficiency using single photon ionization and also from the near zero background nature of the technique.[41]

Suits and coworkers have carried out ion imaging studies of hydrocarbon reactions leading to hydrocarbon radical products with relatively low ionization energies that can be photoionized at 7.9 eV.[45–48] However the ionization energies of most non-metallic free radicals exceeds 7.9 eV (Fig. 2), rendering this method ineffective as a universal detection method except for a small number of select systems.

A number of alternatives to synchrotrons exist for production of VUV and XUV radiation. Perhaps the best known approach, still used in photoelectron spectroscopy of stable molecules, employs conventional discharge lamps.[49] However, the intensities of such lamps are typically too low for detection of products from photodissociation or bimolecular reactions. During the past decade, electron beam or RF powered excimer lamps have been employed for soft VUV photoionization in mass spectrometry studies.[50] The 128 nm emission from an Ar_2 lamp is often used, and commercial versions of such lamps, both pulsed and continuous, are now available. However, intensities are still substantially lower than for synchrotron light sources and only a few discrete VUV wavelengths are available.[50] Laser-induced plasma radiation has also been employed as an alternative to synchrotron radiation for studies of the photoionization spectroscopy of small molecules.[51] Focusing a commercial nanosecond excimer laser on a solid target produces a VUV/XUV quasicontinuum which, when dispersed by a grating, provides continuously tunable nanosecond pulsed radiation with ~1% bandwidth in the 10^9 photons per pulse range.[51] Such intensities are sufficient for photoionization spectroscopy but not for detection of products from crossed beam reactive scattering studies.

The generation of pulsed VUV radiation using nonlinear frequency conversion of UV and visible lasers has been exploited quite extensively over the past two decades. Photoionization cross sections for most atoms and molecules increase sharply above threshold. For example, the ionization energy of phenyl radicals (C_6H_5) is 8.6 eV and the photoionization cross section is 1.3×10^{-17} cm^2 at 9.9 eV (125 nm).[52] Using a pulsed VUV light source under conditions where the number of photons greatly exceeds the number of molecules, ionization of 2.5% of the molecules requires a photon flux of $\sim 2 \times 10^{15}$ cm^{-2}. To achieve 2.5% ionization within a laser diameter of 2 mm, a pulse energy of 0.10 mJ (6×10^{13} photons per pulse) is required.

Third harmonic generation ($\omega_{VUV} = 3\omega_1$) or resonance enhanced four wave mixing ($\omega_{VUV} = 2\omega_1 + \omega_2$) using focused nanosecond pulsed lasers in inert gas (*e.g.* Kr or Xe) cells or pulsed jets is the most well-established method for production of coherent narrow-bandwidth VUV/XUV radiation.[53–57] Generation of 10^{10} photons per pulse is readily achievable. Under favorable cases where phasematching is possible using inert gas mixtures, VUV pulses approaching 10^{12} photons per pulse can be generated in certain wavelength ranges including Lyman-α at 121.6 nm.[23,55] While such intensities are suitable for Rydberg tagging TOF spectroscopy[22–25] or imaging of atomic species,[58] these sources are still too weak for universal product detection in crossed beam experiments.

Experimental and theoretical work by several groups has demonstrated that much higher VUV conversion efficiencies may be obtained using metallic gases such as mercury (Hg) as the nonlinear medium.[59–62] For example, up to 10^{13} photons per pulse near 125 nm (9.9 eV) have been produced by tuning a commercial frequency doubled dye laser to the Hg $6s(^1S_0) \rightarrow 7s(^1S_0)$ two-photon resonance at 312.85 nm and mixing with the residual 625.70 nm radiation in a focused geometry.[59] By instead mixing the 312.85 nm light with tunable light from a second dye laser, the VUV is broadly tunable with maximum conversion efficiencies in the vicinity of Hg Rydberg resonances.[59] To date, most experimental work using Hg has employed tight-focusing conditions where peak intensities are far above those where simple theory can be used to predict

optimum phase matching conditions.[59,60] Under these conditions, saturation and other competing nonlinear processes often limit the degree to which VUV systems can be scaled to higher energies.

Production of VUV pulses with energies in the millijoule range (>5 × 10^{14} photons per pulse) at 130 nm was first proposed by Smith and Alford[61] and then demonstrated experimentally by Muller and coworkers[62] using four-wave mixing of transform-limited unfocused nanosecond pulsed lasers in Hg vapor. This method is most general and efficient if three independent input laser beams are each tuned near Hg resonances at the precise wavelengths where index matching may be achieved. Continuous wave (CW) Lyman-α has also been produced using a variant of this approach.[63] As described in the following sections, we have employed commercially-available nanosecond dye lasers to produce high intensity pulsed VUV at 9.9 eV. This allows "soft universal" photoionization detection of a range of interesting free radical species (Fig. 2).

2. Experimental methods

The experiments were carried out using a rotatable source, fixed detector crossed molecular beams apparatus (Fig. 3).[41] The phenyl beam was produced *via* photolysis of chlorobenzene at 193 nm.[52] A beam of chlorobenzene (Aldrich) (~10 Torr) seeded in ~1800 Torr of H_2 was produced *via* a pulsed piezoelectrically actuated supersonic expansion.[64,65] A pulsed excimer laser (GAM EX-10) operating at 193 nm photolyzed the precursor forming primarily phenyl radicals and chlorine atoms.[52] The laser was mounted to the source assembly and rotated with it thereby maintaining good alignment for all source angles. The output of the excimer laser, which provided ~15 ns pulses (10 mJ), was gently focused to a 6 mm × 2 mm spot directly in front of the orifice of the pulsed valve. For reactive scattering experiments, the phenyl beam ($\langle v \rangle$ = 2200 m s^{-1}, speed ratio = 10) passed through a 2 mm diameter skimmer (Precision Instruments) into the main chamber region, maintained at or below 5 × 10^{-6} Torr. In nonreactive scattering experiments an additional stage of differential pumping was employed with the beam skimmed by a 2 mm diameter skimmer and then further collimated with a square (3 mm × 3 mm) knife-edge defining aperture fabricated using four razor blades. The O_2 beam ($\langle v \rangle$ = 950 m s^{-1}, speed ratio = 12) was generated by pulsed supersonic expansion of a 40% O_2 in He mixture. The N_2 beam ($\langle v \rangle$ = 970 m s^{-1}, speed ratio = 14) was produced using a 40% N_2 in He mixture. The propene (C_3H_6) beam ($\langle v \rangle$ = 1050 m s^{-1}, speed ratio = 12) was produced using a 25% C_3H_6 in He mixture. In all experiments, the molecular beam was collimated by a 2 mm diameter skimmer (Precision Instrument) before entering the main chamber and crossing the phenyl beam at a 90° collision angle. The molecular (O_2, N_2 or C_3H_6) beam was characterized in a separate series of experiments by monitoring its time-of-flight (TOF) distributions on-axis using a slotted chopper wheel with a mass spectrometer detector using electron impact ionization detection. Scattered species travelled 24.1 cm through a series of three apertures and were ionized by a single VUV photon at 9.9 eV in a detector region maintained below 1 × 10^{-9} Torr during the experiment. The resulting positive ions were mass selected using a quadrupole mass filter (Extrel Merlin with 0.75″ pole diameter) and detected using a conversion dynode/electron multiplier operating in pulse counting mode.

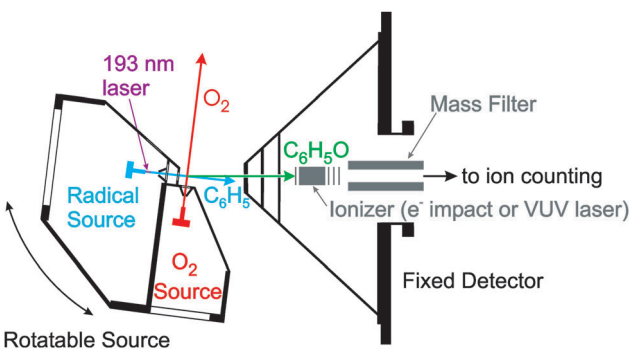

Fig. 3 Schematic of the Cornell fixed detector, rotatable source crossed molecular beams apparatus, configured for studies of the C_6H_5 + O_2 reaction.

Time of flight spectra were generated at a given laboratory angle by scanning the delay of the 9.9 eV light source relative to that of the 193 nm photolysis laser. The laboratory angular distribution was generated by integrating the TOF spectra at each laboratory angle. The TOF spectra were fit using the forward convolution technique, taking as inputs instrumental parameters as well as center-of-mass (CM) distribution functions, namely $P(E)$, the CM translational energy release, and $T(\theta)$, the CM angular distribution, and outputting calculated laboratory TOF and angular distributions.[66] The two CM functions were iteratively adjusted until the calculated TOF and angular distributions matched their experimental counterparts.

2.1 High intensity VUV generation using collimated laser beams

Pulsed VUV light was generated by resonance-enhanced four-wave mixing of collimated lasers in Hg vapor using several different near-resonant schemes (Fig. 4).[67] The simplest approach involved mixing the output of two pulsed dye lasers to generate 9.9 eV photons, $\omega_{VUV} = 2\omega_1 + \omega_2$, with ω_1 = 31 964 cm^{-1} and ω_2 = 15 800 cm^{-1}, in a 1 meter long Hg cell (400 K). In this configuration the 31 964 cm^{-1} light was produced by frequency doubling the output of a 532 nm pumped dye laser (Scanmate 2, DCM laser dye) in a KDP crystal and the 15 800 cm^{-1} light was produced directly from a separate 532 nm pumped dye laser (Scanmate 2, DCM laser dye). We also carried out experiments using three separately tunable input frequencies, $\omega_{VUV} = \omega_1 + \omega_2 + \omega_3$, with $\omega_1 \approx$ 39 200 cm^{-1}, $\omega_2 \approx$ 24 700 cm^{-1} and $\omega_3 \approx$ 15 950 cm^{-1}. The three tunable frequencies were each generated using pulsed nanosecond dye lasers (Scanmate 2). Note that in this case, $\omega_1 + \omega_2$ = 63 928 cm^{-1}, corresponding to the same Hg $6s(^1S_0) \rightarrow 7s(^1S_0)$ two-photon resonance employed in the first approach. A third approach also involved three separate frequencies with ω_1 being the fourth harmonic of a seeded Nd:YAG laser (266 nm), ω_2 tuned so that $\omega_1 + \omega_2$ = 63 928 cm^{-1}, as in the first two cases, and $\omega_3 \approx$ 15 800 cm^{-1}. The use of three separate frequencies for VUV generation

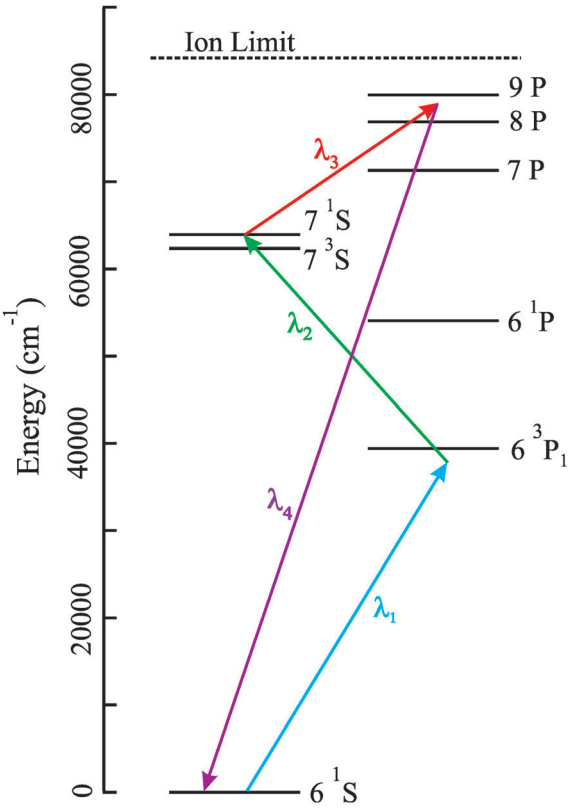

Fig. 4 Scheme for near-triply resonant four-wave mixing in mercury vapor, with some of the relevant mercury atomic states indicated.

produced ~6 × 10^{13} photons per pulse at 9.9 eV.[67] The approaches with 3 distinct input frequencies were found to produce VUV intensities ~2–3 times greater than using two frequencies. Use of three separately-tunable frequencies allowed for increased flexibility in tuning the VUV since index matching changes as the input frequencies change.[61,67] In all of the configurations a single-injection seeded Continuum Powerlite 9030 Nd:YAG laser was used to pump the dye lasers, either with the second (532 nm) or third (355 nm) harmonic.

All input laser beams were aligned spatially and temporally through a 1 m long mercury heat pipe held at ~400 K. A slow flow of helium buffer gas was directed away from the windows at ~10 Torr to protect the optics at each end of the cell from contamination. The VUV beam was spatially dispersed from the UV and visible laser beams by off-axis transmission through a 50 cm MgF_2 lens (ISP Optics). The VUV passed by the edge of a ceramic beam dump mounted on a linear translation stage, while the UV and visible beams (dispersed by a smaller angle) were physically blocked by the ceramic beam dump. The isolated VUV beam then passed through two differentially pumped apertures before arriving at the ionization region of the detector. By employing only one optical element (the 50 cm focal length MgF_2 lens) between the VUV cell and the detector, window losses were minimized.

2.2 Radical beam production

Production of molecular free radicals can be achieved *via* a variety of techniques: photolysis,[39] pyrolysis,[68] electrical discharge,[69] chemical reaction,[70] *etc.* In most of these cases a relatively weak bond of a stable precursor is cleaved to generate the corresponding radical. The weak bond will also often fragment upon ionization using hard (80–100 eV) electron impact, producing the same mass as the radical of interest. Monitoring the radical species itself is often difficult using "universal" mass spectrometric detection. In cases where the spectroscopy of the radical species is known (OH,[16,71] CN,[72–74] CH_3,[18] *etc.*), LIF or REMPI can be used, but as noted earlier, this is generally not the case for many polyatomic free radicals.

By employing "soft" ionization, fragmentation of the parent species is usually reduced or eliminated, allowing for clean detection of the radical species even when looking directly on-axis at the radical beam. This allows for convenient optimization for the production of molecular radicals. As can be seen in Fig. 5 the production of phenyl radicals on-axis from the photodissociation of chlorobenzene is very difficult to optimize using traditional hard electron impact ionization. The chlorobenzene parent fragments substantially to $C_6H_5^+$ (m/z = 77). The absolute signal at m/z = 77 actually decreased when the photolysis laser is turned on due to depletion of the C_6H_5Cl parent molecules, which produce signals at m/z = 77 that are stronger than C_6H_5 radicals themselves. When using "soft" single photon ionization, on the other hand, fragmentation of chlorobenzene to m/z = 77 is negligible and the presence of phenyl radicals is easily observed (Fig. 5), making optimization of the phenyl radical beam quite straightforward. We found that modest photolysis laser powers (~10 mJ per pulse) produced the most intense phenyl radical beams; higher laser powers led to photodissociation of the phenyl radicals. "Soft" ionization also facilitates

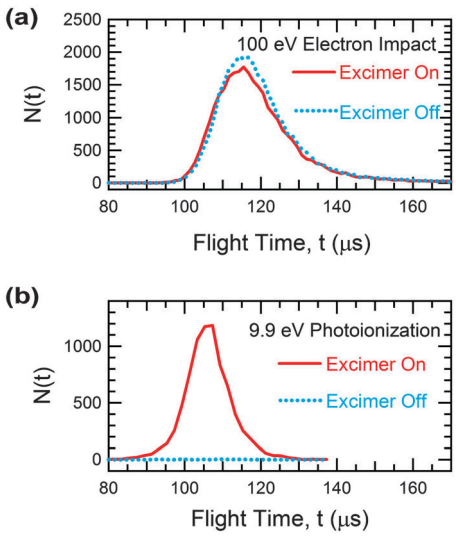

Fig. 5 Time-of-flight spectra recorded at $C_6H_5^+$ (m/z = 77) with C_6H_5Cl beam sampled by mass spectrometer detector directly on-axis (0°). When the 193 nm photolysis laser is off (dotted curve) the beam contains only chlorobenzene molecules and carrier gas. When the 193 nm photolysis laser is on (solid curve), phenyl radicals are produced. (a) Using 100 eV electron impact ionizer, $C_6H_5^+$ signal decreases slightly when laser is on due to photolysis of C_6H_5Cl. (b) Using 9.9 eV photoionization, all signal is attributable to photolytic C_6H_5 with no C_6H_5 signal resulting from fragmentation of C_6H_5Cl.

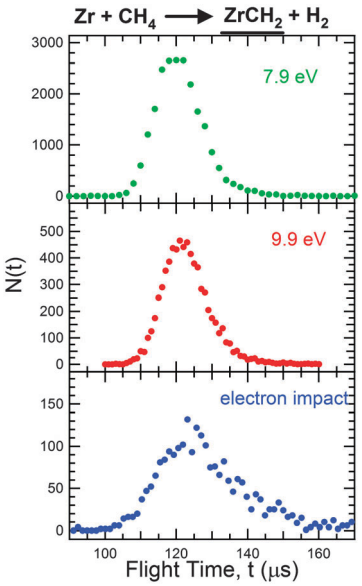

Fig. 6 Time-of-flight distributions at 10° laboratory angle (angle of center of mass of system) monitored at $m/z = 105$ ($ZrCH_2^+$) for $Zr + CH_4 \rightarrow ZrCH_2 + H_2$. The top panel used an F_2 excimer laser at 7.9 eV for single photon ionization. The middle panel employed the 9.9 eV photoionization light source. The bottom panel was monitored using electron impact ionization. Each spectrum recorded by averaging 30 000 laser shots.

observation of impurities which can potentially interfere with detection of the desired product species in molecular beam scattering experiments. The 9.9 eV light source is thus an extremely effective tool for characterizing beams of polyatomic free radicals.

2.3 7.9 eV *vs.* 9.9 eV photoionization

We have examined the reaction $Zr + CH_4 \rightarrow ZrCH_2 + H_2$ to compare product detection using our new 9.9 eV light source with the use of an F_2 excimer laser (GAM Laser EX100HF), 1.0 mJ per pulse (8×10^{14} photons per pulse) at 7.9 eV, and with electron impact ionization at 100 eV. The TOF spectra at the center of mass angle measured using each method is shown in Fig. 6. The signal levels observed using the 7.9 eV light source were approximately a factor of five greater than observed using the 9.9 eV light source, which in turn was about a factor of five greater than observed using 100 eV electron impact. The signal to noise ratios using photoionization were substantially greater than that obtained using 100 eV electron impact ionization. The 9.9 eV light source opens up the opportunity to study a variety of systems that could not be studied using the 7.9 eV light source, including catalytically-relevant transition metal reactions (Pt, Pd, *etc.*) with hydrocarbons, as well as many reactions producing molecular free radicals (Fig. 2). We now turn our attention to some phenyl radical reactions studied using the 9.9 eV light source.

3. Crossed molecular beam reactions of phenyl radicals

Phenyl radicals (C_6H_5) are important in combustion because they are reaction intermediates in the oxidation of aromatic species.[10,27] Phenyl radical reactions with unsaturated hydrocarbons lead to production of polycyclic aromatic hydrocarbons (PAH), which in turn lead to soot formation. The primary mechanism for PAH formation is thought to occur *via* the "hydrogen-abstraction–acetylene-addition" (HACA) mechanism,[10,27,75] in which phenyl radicals are produced and then add to unsaturated hydrocarbons. The reaction products following addition can undergo hydrogen atom abstraction forming a new radical species that can then add to another unsaturated hydrocarbon. By repeating this process, larger PAH can be generated *via* stepwise addition of smaller hydrocarbons.[75] Understanding branching ratios and reaction mechanisms of phenyl radical reactions is important in modeling the formation of PAH and soot particles. Here we present some examples using the "soft" photoionization technique at 9.9 eV to study reactions of phenyl radicals with molecular oxygen (O_2) and propene (C_3H_6).

3.1 Nonreactive and reactive collisions of $C_6H_5 + O_2$

The reaction of C_6H_5 with O_2 can compete directly with other processes that lead to the formation of polycyclic aromatic hydrocarbons (PAH), and, depending on the reaction products, potentially suppress the formation of soot.[10,27] Therefore, understanding the oxidation of C_6H_5 is critical to modeling the growth of PAH and soot particles.

When a phenyl radical encounters an O_2 molecule, phenylperoxy (C_6H_5OO) intermediates (located $\sim$200 kJ mol^{-1} below the reactants) can be formed. These intermediates can decompose to a variety of new reaction products or back to reactants.[76] However, elastic and inelastic nonreactive collisions also occur, without formation of C_6H_5OO. By studying the nonreactive scattering of phenyl radicals with molecular oxygen, we can gain insight into such nonreactive collisions. The C_6H_5 TOF spectra for nonreactive scattering were obtained by subtracting TOF spectra with the O_2/N_2 beam off from TOF spectra with the O_2/N_2 beam on at various angles. The nonreactive TOFs for phenyl radicals scattering from O_2 and N_2 are shown in Fig. 7. Nonreactive scattering of C_6H_5 from both O_2 and N_2 can be fit with identical $P(E)$ and $T(\theta)$ distributions (Fig. 8). The similarity between the nonreactive scattering from both O_2 and N_2 and the lack of intensity in the backward direction, which would correspond to long-lived C_6H_5OO complexes decaying back to $C_6H_5 + O_2$, implies that most C_6H_5OO intermediates decay to new reaction products and not back to reactants.[77] The absence of background from fragmentation of chlorobenzene producing $C_6H_5^+$ at $m/z = 77$ facilitates the study of nonreactive scattering even at angles very close to the phenyl radical beam.

Calculations indicate that O–O bond fission in C_6H_5OO producing $C_6H_5O + O$ (^3P) has no potential energy barrier above the reaction endoergicity, D_0 (C_6H_5O–O) = 156 kJ mol^{-1}. The low barrier for production of $C_6H_5O + O$ is consistent with our finding that most of the C_6H_5OO intermediates decay to new reaction products. The other energetically accessible channels require multiple isomerization steps.[76] Consequently, the lifetimes of the C_6H_5OO intermediates, which are largely determined by the rate of O–O bond fission

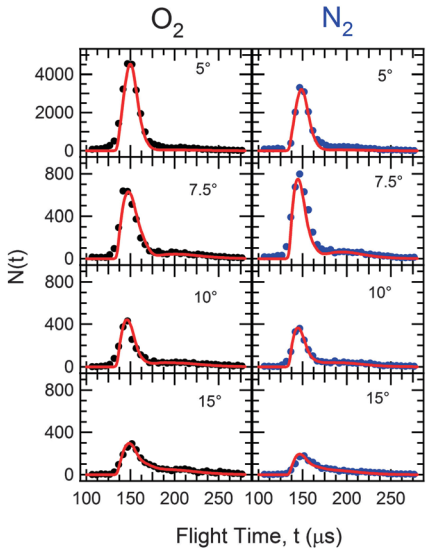

Fig. 7 Time-of-flight distributions (m/z = 77) at the indicated laboratory angle for non-reactive scattering of phenyl radicals from O_2 (left panel) and N_2 (right panel). Points are the experimental data. Solid lines are fits to the data using the CM distributions shown in Fig. 8. The same CM distributions were used to fit the non-reactive scattering of phenyl radicals from both O_2 and N_2. All time-of-flight distributions are normalized to the same number of laser shots.

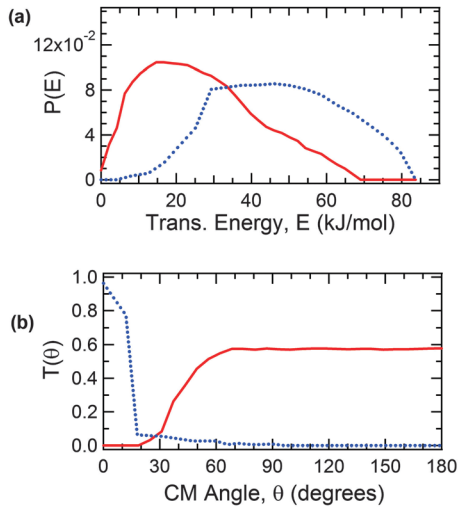

Fig. 8 Center-of-mass distributions (m/z = 77) used to fit the non-reactive scattering of phenyl radicals from O_2 and N_2 (same distributions used for both O_2 and N_2). Both a forward scattered component (dotted line) and a sideways/backward scattered component (solid line) were used to fit the data. The branching ratio between the forward component and the sideways/backward component was found to be 4 : 1.

in C_6H_5OO, play a critical role in determining branching ratios in this reaction.

In 2007 Kaiser and coworkers carried out a crossed molecular beams study of the C_6H_5 + O_2 reaction under single collision conditions using 80 eV electron impact detection.[78] Employing a pyrolytic pulsed phenyl radical source using nitrosobenzene as the precursor, the reaction at a nominal collision energy of 107 kJ mol^{-1} was found to proceed to C_6H_5O + O *via* a direct mechanism with very short lifetimes of C_6H_5OO intermediates.[78] In 2012 Kaiser and coworkers carried out another study of C_6H_5 + O_2, this time using a photolysis of chlorobenzene as their phenyl radical source at a collision energy of 38 kJ mol^{-1}.[79] At the lower collision energy they found that long-lived C_6H_5OO intermediates decayed to C_6H_5O + O products.[79] We examined the reaction using a photolytic source of phenyl radicals at an intermediate collision energy (64 kJ mol^{-1}) using the pulsed 9.9 eV VUV photoionization method.[80] Time-of-flight (TOF) spectra were recorded at various laboratory angles for m/z = 93, $C_6H_5O^+$, and m/z = 65, $C_5H_5^+$. We carefully searched for signal attributable to the other major product channels predicted by the calculations of Tokmakov *et al.*[76] These included m/z = 108, $C_6H_4O_2$ (IP = 9.6 (*ortho*-); 9.9 eV (*para*-)) from the $C_6H_4O_2$ + H channel, and m/z = 81, C_5H_5O (IP unknown) from C_5H_5O + CO.[81] In addition, there are two potential sources of C_5H_5 products. Unimolecular rearrangement of C_6H_5OO can lead to formation of C_5H_5 + CO_2. Alternatively, if formed with sufficient internal energy, C_6H_5O from O–O bond fission of C_6H_5OO can undergo secondary decomposition over a large potential energy barrier to form C_5H_5 + CO.[82] While we did observe signal at m/z = 65 ($C_5H_5^+$), it was nearly superimposable with that obtained at $C_6H_5O^+$, indicating that the $C_5H_5^+$ signal primarily comes from fragmentation of C_6H_5O during photoionization. This is consistent with previous observations in studies of the photodissociation of nitrobenzene,[83] phenol[84] and anisole[85] in which single photon ionization of C_6H_5O products near 10 eV produces parent ions ($C_6H_5O^+$) as well as $C_5H_5^+$ daughter ions. Each TOF spectrum at m/z = 93, shown in Fig. 9, consists of ~30 000 laser shots, corresponding to ~20 min of data collection time. The solid line fits to the laboratory angular distribution and TOF spectra were simulations of the

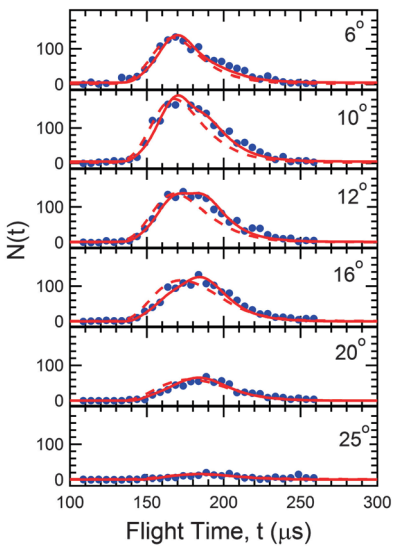

Fig. 9 Time-of-flight distributions (m/z = 93) monitoring the reaction C_6H_5 + O_2 → C_6H_5O + O at the indicated laboratory angles. Points are experimental data. Solid line is best fit to the data using the center-of-mass distributions shown as solid lines in Fig. 10. Dotted line was calculated using $T(\theta)$ shown as dotted line in Fig. 10. Adapted from ref. 80.

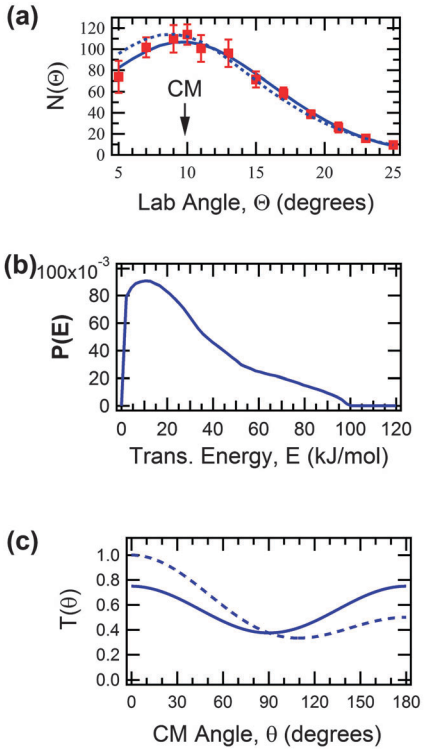

Fig. 10 Laboratory and center-of-mass distributions (m/z = 93) for the reaction $C_6H_5 + O_2 \rightarrow C_6H_5O + O$. (a) Laboratory angular distribution. Points are experimental measurements with 1 σ error bars. Solid line is best fit to the experimental data using the center-of-mass distributions shown as solid lines in parts (b) and (c). Dotted line corresponds to $T(\theta)$ shown as dotted line in (c). (b) Best fit center-of-mass translational energy release. (c) Best fit center-of-mass angular distribution shown as solid line. Adapted from ref. 80.

experimental data performed using the forward convolution technique. The laboratory angular distribution and best fit center-of-mass distributions are shown in Fig. 10. The best fit center-of-mass angular distribution is forward-backward symmetric.[80]

A forward–backward symmetric angular distribution is characteristic of a reaction involving C_6H_5OO collision complexes with lifetimes of at least several rotational periods. Using the largest moment of inertia of C_6H_5OO the rotational period is 6.4 ps for J = 5 and 1.7 ps for J = 10.[76] In agreement with Kaiser and coworkers, we were only able to detect the C_6H_5O + O channel in the reaction of C_6H_5 with O_2.[78–80] Our CM translational energy distribution $P(E)$, and CM angular distribution $T(\theta)$, are consistent with the conclusions from experiments carried out at the lower collision energies.[79] We find that the $P(E)$ peaks at low translational energy release,[80] $\sim$10 kJ mol^{-1}, which is much lower than $\sim$75 kJ mol^{-1} reported at the higher collision energy.[78] Our conclusion that the reaction is dominated by formation of long lived collision complexes at a mean collision energy of 64 kJ mol^{-1}[80] is consistent with the conclusions derived from experiments at low collision energies.[79] However, we have not observed any evidence for the onset of a direct reaction mechanism producing forward-scattered C_6H_5O even at collision energies as high as 97 kJ mol^{-1}.[86]

3.2 Competing pathways in the reaction $C_6H_5 + C_3H_6$ (propene)

Previous studies of the reactions of a wide range of unsaturated systems (including propene) with phenyl radicals have been carried out in Kaiser's group using the method of crossed molecular beams with 80 eV electron impact detection.[29,30,87] In order to assess the performance of our apparatus employing pulsed VUV photoionization detection, we studied the propene reaction using the same photolytic C_6H_5 source employed in our study of the C_6H_5 + O_2 reaction. Since electron impact ionization is perhaps the best-tested approach in the field, it is important to characterize our new method on a system that has already been studied in detail before embarking on new systems. In the first series of experiments by Kaiser's group, carried out at high collision energies, the only observed product channel was H atom elimination, forming C_9H_{10}.[29,87] For the propene reaction, this was taken as evidence that reaction occurred exclusively by addition of the phenyl radical to the 1-carbon atom (*i.e.*, to the CH_2 group) rather than to the methyl substituted carbon atom. This behavior was attributed to steric effects and a propensity for the electron deficient phenyl radical to attack the carbon with a greater electron density.[29] From the signal to noise calculations, it was concluded that the CH_3 elimination channel, forming C_8H_8, cannot account for more than 10% of the total reaction cross section.[29] In more recent work, carried out at a lower collision energy, the CH_3 elimination channel producing C_8H_8 was observed, in addition to H-atom elimination channel producing C_9H_{10}.[30] However, due to substantial fragmentation of the C_9H_{10} to m/z = 104 the C_8H_8 product TOF distributions were subject to significant interference.[30]

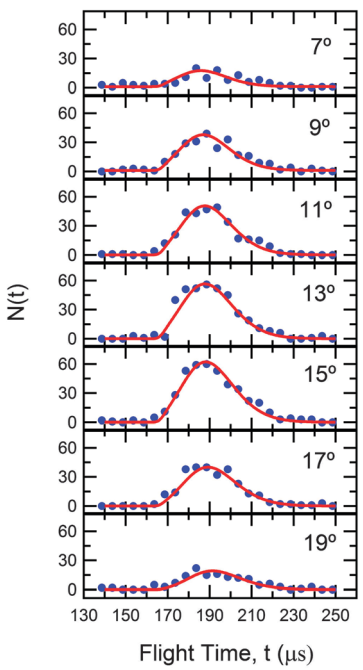

Fig. 11 Time-of-flight distributions (m/z = 118) monitoring the reaction C_6H_5 + $C_3H_6 \rightarrow C_9H_{10}$ + H at the indicated laboratory angles. Points are experimental data. Solid line is the best fit to the data using the center-of-mass distributions shown in Fig. 12.

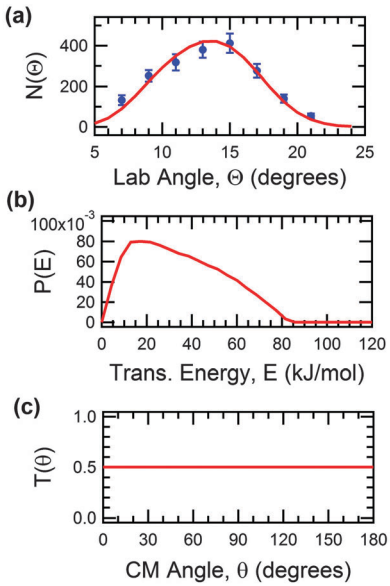

Fig. 12 Laboratory and center-of-mass distributions (m/z = 118) for the reaction $C_6H_5 + C_3H_6 \rightarrow C_9H_{10} + H$. (a) Laboratory angular distribution. Points are experimental measurements with 1 σ error bars. Solid line is best fit to the experimental data using the center-of-mass distributions shown in parts (b) and (c). (b) Best fit center-of-mass translational energy release. (c) Best fit center-of-mass angular distribution.

We studied the title reaction at collision energy of 84 kJ mol^{-1}, which is in between that used in the previous studies. Not surprisingly, we observed H atom elimination producing C_9H_{10}, which was monitored at its parent mass, m/z = 118 (Fig. 11). The laboratory angular distribution and the CM distribution functions for the C_9H_{10} + H product channel are shown in Fig. 12. We also observed strong signal at m/z = 104, corresponding to C_8H_8 resulting from methyl radical elimination, *i.e.*, $C_6H_5 + CH_2CHCH_3 \rightarrow C_6H_5CHCH_2 + CH_3$ without any fragmentation from the H-atom elimination channel products (Fig. 13). The laboratory angular distribution and the CM distribution functions for the C_8H_8 + CH_3 product channel are shown in Fig. 14. Representative TOF spectra for the C_9H_{10} + H channel (Fig. 11) and for the C_8H_8 + CH_3 channel (Fig. 13) were each accumulated using ~30 000 laser shots, corresponding to about 20 minutes of averaging at each angle. We find that the absolute signal level at a given angle for the C_8H_8 channel (CH_3 elimination) is nearly as large as that for H atom elimination. Both channels involve long-lived reaction intermediates that decay over modest barriers. The Newton sphere for the C_9H_{10} channel is very small (due to the light H atom counterfragment), so products are constrained to a very small laboratory angular range (Fig. 1). The C_8H_8, on the other hand, recoils from a heavier counterfragment, CH_3, and is scattered over a relatively large Newton sphere (Fig. 1). The similar signal levels for both C_9H_{10} and C_8H_8 products suggest that C_8H_8 formation is significant in the $C_6H_5 + C_3H_6$ reaction.

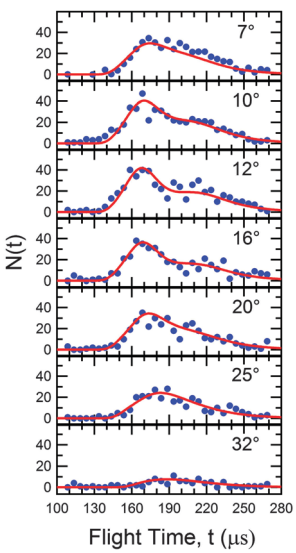

Fig. 13 Time-of-flight distributions (m/z = 104) monitoring the reaction $C_6H_5 + C_3H_6 \rightarrow C_8H_8 + CH_3$ at the indicated laboratory angles. Points are experimental data. Solid line is the best fit to the data using the center-of-mass distributions shown in Fig. 14.

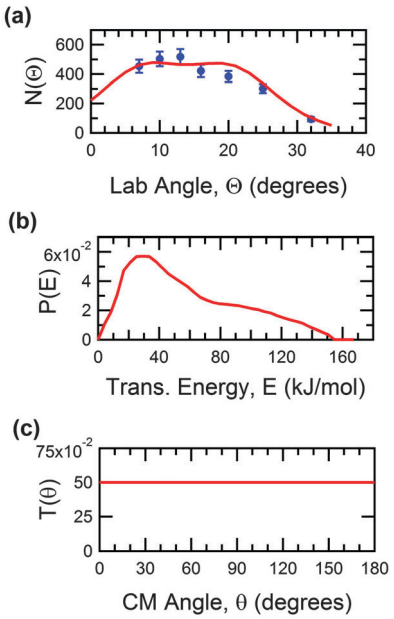

Fig. 14 Laboratory and center-of-mass distributions (m/z = 104) for the reaction $C_6H_5 + C_3H_6 \rightarrow C_8H_8 + CH_3$. (a) Laboratory angular distribution. Points are experimental measurements with 1 σ error bars. Solid line is best fit to the experimental data using the center-of-mass distributions shown in parts (b) and (c). (b) Best fit center-of-mass translational energy release. (c) Best fit center-of-mass angular distribution.

3.3 Determination of product branching ratios

To be a truly "universal" detection scheme, the relative detection sensitivity for all potential products must be well defined. The observed signal levels for two different reaction products depend upon the ionization cross sections and reaction kinematics.[2,88] It is well established that electron impact ionization cross sections for molecules are proportional to the square root of the molecular polarizabilities.[2,89] Molecular polarizabilities are usually approximated as being equal to the sum of atomic

polarizabilities.[2] Data measured using electron impact ionization is typically analyzed using calculated ionization cross sections and measured fragmentation patterns.[2] Photoionization cross sections cannot be estimated in a similar manner, and must be measured in order to accurately determine product branching ratios.[90,91] Relative photoionization cross sections for stable molecules can be determined by photoionization detection using molecular beams containing the molecules of interest.[91] Relative and absolute photoionization cross sections for molecular radical species can be determined by generating the molecular radical in photodissociation experiments and comparing the detection sensitivity of the molecular radical species with its momentum matched atomic recoil partner, which has a known photoionization cross section.[52,92]

We have carried out experiments using beams of C_8H_8 (styrene) (Aldrich) and C_9H_{10} (α-methyl styrene) (Aldrich) with both electron impact and 9.9 eV photoionization. By comparing the signal levels from nonreactive scattering of C_8H_8 or C_9H_{10} at a few different angles using electron impact and photoionization, we find that the photoionization cross section is the same for the two species within our experimental uncertainty. This is not surprising as molecules belonging to a particular class (alkane, alkene, monoaromatic species, *etc.*) often have similar photoionization cross sections at photon energies well above their ionization energies.[93,94] We also anticipate that different possible C_9H_{10} isomers will all also have similar photoionization cross sections to α-methyl styrene, as all of the predicted isomers have ionization energies that are within 0.2 eV of each other.[81] When we take into account the differing kinematics of the product channels, assume that no fragmentation of the parent ion exists at 9.9 eV photoionization and assume that the photoionization cross sections for all H-atom elimination products are equal to that of α-methyl styrene, we find that at a collision energy of 84 kJ mol^{-1} the methyl-elimination channel is dominant by 10 to 1 over the H-atom elimination channel.

Another important consideration in studies of bimolecular reactions or photodissociation is the dependence of the photoionization cross section on the parent molecule's vibrational energy. Several detailed studies have been carried out to address this issue.[95–97] Not surprisingly, the internal energy of the neutral plays the most important role in experiments where photoionization is carried out near threshold.[95–97] Most notably, if the photon energy lies below the vertical ionization energy of the neutral to be detected,[95,96] the detection sensitivity for vibrationally cold neutrals may be zero. In situations where a significant geometry change occurs upon ionization, parent vibrational energy could be very effective in promoting ionization under such circumstances. Similarly, even at photon energies well above threshold, the detection sensitivity for different internal states of a given species depends on details (such as Franck–Condon factors) that must be considered explicitly for the molecules of interest.[97] Recent experiments have found that when molecules are ionized using single photon ionization at or above the vertical ionization threshold, ionization cross sections are relatively independent of internal energy.[97–99] The use of 9.9 eV radiation is well above the ionization energies of all products in the $C_6H_5 + C_3H_6$ reaction.[81] Therefore, we expect no vibrational energy dependence on product detection sensitivity.

4. Discussion

With the notable exception of experiments employing 7.9 eV photoionization using excimer lasers,[41–48] soft universal photoionization detection in crossed beams experiments has previously been restricted to experiments conducted at dedicated synchrotron facilities.[34–40] At the present time, however, only one such crossed beams apparatus is in operation worldwide.[35,37,38] Therefore, our efforts in developing intense VUV light sources employing tabletop commercial lasers should considerably increase the range of chemical systems that can be studied by researchers outside of dedicated synchrotron facilities. High intensity VUV sources of this kind should also be of great interest for studies of VUV photodissociation, and in more applied areas such as materials processing.

For product detection using synchrotron photoionization or electron impact ionization, the continuous nature of the detector is best exploited using *continuous* molecular beams.[100] By modulating the products using a slotted chopper wheel, product velocity distributions are measured by time of flight. Since elementary reactions between stable closed-shell molecules are rare,[101] *in situ* production of free radicals is a fundamental requirement for such experiments, necessitating the use of *continuous* discharge[12,102] or pyrolysis[68] methods. As already noted, Casavecchia's group has pioneered both methods for studies of a wide range of important chemical systems using "soft" electron impact ionization, as summarized in comprehensive review articles.[11,12]

At Berkeley's Advanced Light Source, the first crossed beams apparatus employing synchrotron photoionization detection was available to the dynamics community between 1994 and 2004.[34] This apparatus was used extensively for studies of molecular photodissociation, most notably by the groups of Butler[96,103] and Neumark.[52,95,104] During this period, however, only three reactive scattering studies were published: $Cl + C_3H_8$ (propane) $\rightarrow C_3H_7 + HCl$,[40] $Cl + C_5H_{12} \rightarrow C_5H_{11} + HCl$[36] and $^1CH_2 + C_2H_2 \rightarrow C_3H_3 + H$.[39] In the Cl atom studies, a continuous pyrolysis source was well-matched to the continuous nature of the detector.[36,40] Since a large fraction of Cl_2 can be dissociated at a moderate temperature, and because secondary reactions of the radicals within the nozzle are not significant, the product signal to noise ratios were quite high.

In the studies of reactions of electronically excited $^1CH_2$ at the ALS, photolysis of ketene using a 308 nm pulsed excimer laser (100 Hz) was employed.[39] For production of certain radical species, particularly molecular free radicals, photodissociation of a stable precursor is an extremely attractive approach. To achieve radical number densities sufficient for reactive scattering studies, photodissociation typically requires precursor molecules with sufficient cross-sections ($>5 \times 10^{-19}$ cm^2 per molecule) for photodissociation producing the radical of interest. Lasers must be sufficiently powerful to photolyze a significant fraction of precursor molecules.

This usually necessitates UV light from pulsed excimer (*e.g.*, 193 nm or 248 nm) or Nd:YAG lasers (*e.g.*, 355 or 266 nm). In such cases the pulse repetition rates are typically 10–200 Hz range.[100] Pulsed molecular beams offer advantages over continuous beams by facilitating the production of higher peak beam intensities with narrower velocity and internal energy distributions through the ability to use higher backing pressures.[100]

In many cases, the internal state distributions of photolytic free radical beams can be much colder than is possible using pyrolysis. For example, photodissociation of HNO_3 produces OH primarily in $v = 0$, and the OH rotational distribution is cooled upon supersonic expansion.[23] Since D_0 (HO–NO_2) is only 199 kJ mol^{-1},[105] flash pyrolysis would seem to be an attractive approach for producing intense beams of OH radicals.[68] However, since high nozzle temperatures are required, and since vibrational energy is in general not cooled efficiently upon supersonic expansion,[106] substantial vibrational excitation is anticipated for such radical beams. For example, assuming a temperature of 1800 K, the fraction of OH in $v = 1$ (corresponding to 3700 cm^{-1} of internal energy) is calculated to be >5%. Our experimental measurements of an OH beam generated in this manner are consistent with these calculations. For reactive scattering studies where narrow distributions of reactant internal energies are highly desirable, such levels of vibrational excitation renders pyrolysis much less desirable than photolysis in the case of OH production.

The fundamental mismatch in duty cycle between *pulsed* photolytic beams and *continuous* detection methods such as electron impact ionization or synchrotron photoionization represents a significant experimental limitation. Using a 100 Hz photolytic source in an apparatus of this type, product TOF distributions typically arrives within a time window of 150 μs or less. Therefore, the duty cycle of the detector is typically no more than 1.5% (150 μs per pulse × 100 pulses per s = 0.015 s/s = 1.5%). Thus, although a third-generation synchrotron produces $\sim 10^{16}$ photons per s, at most 1.5×10^{14} photons per s are actually usable when one or more components of the experiment are pulsed. Also, until the ''top off mode'' was introduced in 2003 at Berkeley's advanced light source, VUV intensities decayed over a several hour period, making normalization difficult.[107] The limitations on maximum pulse rates for high power UV lasers represented a significant inherent limitation to the use of the Berkeley apparatus in crossed beams experiments. While photodissociation experiments are also inherently pulsed (due to the need for a UV photolysis laser), the much larger signal levels inherent to photodissociation experiments (a factor of 10 or more) easily compensated for the duty cycle issue. The unique ability provided by the synchrotron, to tune the photon energy just above threshold for photoionization made this apparatus extremely valuable in a range of studies.[107–110]

In 2002, a new crossed beam apparatus was commissioned at the Taiwan Synchrotron Light Source.[35] Although in many ways similar in design to the Berkeley machine, three notable improvements were made. First, the distance between the beam crossing region and photoionization region of the detector was reduced from 15 cm to 10 cm, leading to a factor of 2.25 increase in signal levels. Also, a quadrupole mass filter with larger pole diameter (1.25″ instead of 0.75″) was employed, increasing the ion transmission by a factor of ~ 2.[35] Finally, a new generation of pulsed valves with very short opening time has made it possible to significantly increase peak beam densities.[111] Collectively, these improvements have a major impact, opening up a wide range of studies not feasible using the Berkeley machine. Currently, this apparatus represents the state of the art in the field.

In our comparison of the use of pulsed photoionization to continuous electron impact ionization detection in transition metal-hydrocarbon chemistry, considerably higher signal to noise ratios were obtained using photoionization.[41] However, a significant experimental constraint in experiments using pulsed VUV photoionization with a fixed mass spectrometric detector is that only a single velocity and product scattering angle is probed at a given laser delay. To map out the product velocity distribution at a given laboratory angle, the delay of the photoionization laser relative to time zero for the reaction must be scanned. Typically such scans cover about 20–30 channels at 5 μs per channel. Due to VUV pulse intensity fluctuations, this produces statistical ''noise'' in the TOF distributions. While it is possible to normalize for long-term drifts in the VUV pulse energies, normalizing for shot to shot intensity fluctuations is difficult. Furthermore, obtaining product angular distributions requires that the angle of the two beams relative to the fixed detector must be rotated. In typical cases, 6–15 different detector angles must be measured in a given experiment.

Ion imaging methods are widely-touted as being superior to ''conventional'' crossed beam experiments because they provide the opportunity to record the entire product angular and velocity distribution in each laser shot, corresponding to a large (factor of >200) multiplexing advantage.[112] Therefore, one might anticipate that ion imaging using pulsed 9.9 eV photoionization could outperform the use of a conventional rotatable source-fixed detector apparatus. As already noted, Suits has studied a number of systems using this method utilizing a 7.9 eV excimer laser.[45–48] Honma and coworkers have recently employed imaging in reactions of transition metal atoms with oxidants such as O_2.[113] Such reactions have large cross sections and are amenable to ionization schemes employing near-UV lasers.[113] For such cases, the molecular species of interest can be ionized selectively with high efficiency and the probability for ionization of reactant molecules or other products is very small. On the other hand, for many studies, the use of *non-resonant* VUV ionization coupled with ion imaging detection is likely to be complicated by photodissociation of molecules in the interaction region[45] or from bimolecular reactions of ions produced by the VUV.[114] In several ion imaging studies by Suits and coworkers, products scattered into certain areas of the Newton circle could not be included in the analysis, leading to fundamental limitations in the range of angles that can be analyzed.[45] In Rydberg tagging experiments carried out in our laboratory, similar issues have frequently arisen. For example, in reactions involving hydrocarbon molecules, the H atom

product is probed by Rydberg TOF spectroscopy. In this case, pulsed VUV at Lyman-α at 121 nm is used to pump the 1s → 2p transition, and then a second laser promotes the H atoms to $n \sim 40$. Since hydrocarbons absorb strongly at 121 nm producing H atoms, this represents an unwanted source of background signal that may be difficult to avoid. Yang has proposed Rydberg tagging studies utilizing a rotatable source machine where the UV and VUV lasers are not located directly at the crossing region as a potential solution to this issue.[25] In this case, careful consideration of the density to flux transformation will be essential to ensure that product kinetic energy release distributions are accurate. We are currently exploring the use of near-transform limited lasers for generation of VUV for detection of O atoms in Rydberg tagging experiments. In this case, the use of very narrowband radiation may increase the contrast ratio between atomic excitation (with narrow lines) and photolysis (broad lines).

Our approach using "soft" single photon pulsed ionization allows the product molecules to drift to a triply differentially pumped detector (10^{-10} Torr) before ionization, spreading out according to their velocities. In contrast to ion imaging or Rydberg tagging experiments where VUV is introduced into the high-pressure molecular beam crossing region, no interference from photodissociation or ion–molecule reactions is observed. As illustrated above, the very high ionization efficiency and very low background count rates lead to quite high signal to noise ratios in our experiment. However, the need to scan the laser delay to measure product TOF distributions represents the key remaining limitation in our current implementation of soft photoionization in crossed beams reactions. To overcome this, we are currently developing the use of *coaxial* VUV photoionization detection. As illustrated in Fig. 15, the use of a fixed detector geometry makes it relatively straightforward to introduce the ionization laser along the detector axis in a counterpropagating geometry. The neutral products from bimolecular reactions drift from the interaction region with their nascent velocity distributions, with a small fraction passing through a series of apertures. Rather than ionizing a 2–3 mm length of the neutral distribution using the crossed-beam configuration of Fig. 3, the packet of neutral molecules is allowed to spread out according to their neutral velocities. At a suitable VUV laser delay, the entire column of neutrals is photoionized by the VUV pulse within a 33 cm long ion guide. Since a light electron is ejected, photoionization does not lead to an appreciable velocity perturbation, and the positive ion is then mass filtered and detected as usual. Photodissociation, if it occurs, leads to ejection of photofragments from the detector axis and will not produce significant background signals. The great advantage of this approach is that the *entire* packet of neutrals is ionized in each laser pulse, rather than a 2–3 mm long segment. The anticipated increase in signal to noise ratio is very large, and will depend upon the specific kinematics of the system under study. The calculated lower limit to the improvement is based on the fact that it will no longer be necessary to scan the VUV laser delay over ~30 channels. The upper limit corresponds to the fact that ionization will occur over a 33 cm pathlength, rather than in a 3 mm pathlength as in the orthogonal (crossed beam) configuration. We thus anticipate increases in signal to noise ratios of a factor of 30–100.

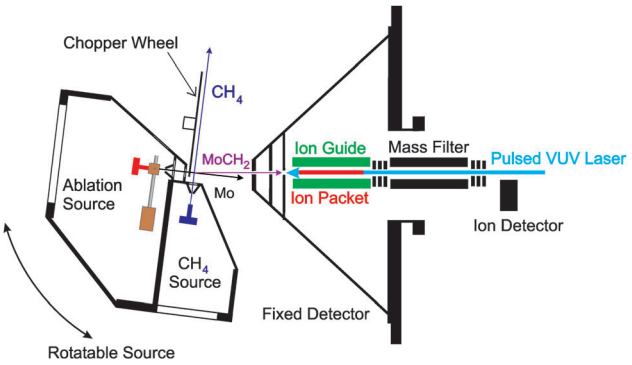

Fig. 15 Crossed beams apparatus with coaxial photoionization detection. Neutral products drift from crossing region through several apertures into ion guide region where they are photoionized by a counterpropagating VUV laser beam. Ions are then mass filtered and detected. The entire velocity distribution is recorded for each laser shot.

The primary challenge in implementing the coaxial ionization method is primarily of a technical nature. One needs to ensure that the entire packet of neutrals is detected with constant (or at least known) sensitivity. We are presently characterizing this approach using a fixed beam apparatus and hope to be able to introduce this method to crossed beam studies in the near future. The most notable improvement will result from the much larger signal levels and the elimination for the need to scan the delay of the detection laser. Since the number of photons is much greater than the number of absorbing molecules, the VUV intensity is constant along the beam axis so no correction for absorption is required.

Our present approach for VUV generation using unfocussed laser beams is most efficient at wavelengths near 125 nm, corresponding to photon energies of ~9.9 eV. While this method can be extended to somewhat higher photon energies, a fundamental constraint is that the transmission of light through MgF_2 and LiF optics decreases sharply at shorter wavelengths, falling to zero at $\lambda < 104$ nm for LiF. To overcome this limitation, we are currently developing techniques to extend the wavelength range into the XUV ($\lambda < 110$ nm) by using resonance enhanced four-wave mixing of focused laser beams in Hg vapor produced by laser vaporization at room temperature.[115] In this way, a windowless configuration can be employed. Furthermore, by using noncollinear phasematching,[116] the need for dispersive elements to separate the XUV from the residual UV beams is eliminated. By combining this approach with the use of coaxial photoionization, we expect that we will be able to use pulsed photoionization for detecting many chemically interesting species with ionization energies up to 12 eV.

5. Conclusions

The development of high-intensity pulsed VUV light sources based on nonlinear frequency conversion of commercial lasers makes it possible to carry out "universal" soft photoionization

detection without the need for synchrotron light sources. The ability to unambiguously identify competing product channels, and the possibility of isomer specific detection, makes VUV photoionization particularly promising.[110] Clearly, the development of new experimental techniques, combined with strong theoretical support, will in the future make it possible to unravel the dynamics of increasingly complex chemical reactions involving polyatomic free radicals.

Acknowledgements

This research was supported by the National Science Foundation under Grant CHE-0809622 (transition metal-hydrocarbon chemistry) and by the Office of Science, U.S. Department of Energy, under Grant DE-FG02-00ER15095 (free radical combustion chemistry). We thank David Proctor for early work on the development of VUV generation using collimated laser beams. The authors thank Ralf Kaiser and Alex Mebel for valuable discussions and suggestions about phenyl radical reactions, and Mark Johnson for suggestions concerning coaxial photoionization detection.

References

1 X. Yang, *Annu. Rev. Phys. Chem.*, 2007, **58**, 433.
2 Y. T. Lee, in *Atomic and Molecular Beam Methods*, ed. G. Scoles, Oxford University Press, New York, 1988, vol. 1, pp. 551–568.
3 R. D. Levine, *Molecular Reaction Dynamics*, Cambridge University Press, Cambridge, 2005.
4 Y. T. Lee, *Science*, 1987, **236**, 793.
5 D. R. Herschbach, *Angew. Chem., Int. Ed. Engl.*, 1987, **26**, 1221.
6 J. C. Polanyi, *Angew. Chem., Int. Ed. Engl.*, 1987, **26**, 952.
7 K. Liu, *J. Chem. Phys.*, 2006, **125**, 132307.
8 P. Casavecchia, N. Balucani and G. C. Volpi, *Annu. Rev. Phys. Chem.*, 1999, **50**, 347.
9 S. Liu, C. Xiao, T. Wang, J. Chen, T. Yang, X. Xu, D. H. Zhang and X. Yang, *Faraday Discuss.*, 2012, **157**, 101.
10 J. A. Miller, M. J. Pilling and J. Troe, *Proc. Combust. Inst.*, 2005, **30**, 43.
11 N. Balucani, G. Capozza, F. Leonori, E. Segoloni and P. Casavecchia, *Int. Rev. Phys. Chem.*, 2006, **25**, 109.
12 P. Casavecchia, F. Leonori, N. Balucani, R. Petrucci, G. Capozza and E. Segoloni, *Phys. Chem. Chem. Phys.*, 2009, **11**, 46.
13 Y. T. Lee, J. D. McDonald, P. R. LeBreton and D. R. Herschbach, *Rev. Sci. Instrum.*, 1969, **40**, 1402.
14 D. M. Neumark, A. M. Wodtke, G. N. Robinson, C. C. Hayden and Y. T. Lee, *J. Chem. Phys.*, 1985, **82**, 3045.
15 B. Fu, Y.-C. Han, J. M. Bowman, F. Leonori, N. Balucani, L. Angelucci, A. Occhiogrosso, R. Petrucci and P. Casavecchia, *J. Chem. Phys.*, 2012, **137**, 22A532.
16 J. L. Kinsey, *Annu. Rev. Phys. Chem.*, 1977, **28**, 349.
17 K.-W. Kang, M.-J. Park and J.-H. Choi, *Phys. Chem. Chem. Phys.*, 2011, **13**, 8122.
18 K. Liu, *Phys. Chem. Chem. Phys.*, 2007, **9**, 17.
19 D. Townsend, W. Li, S. K. Lee, R. L. Gross and A. G. Suits, *J. Phys. Chem. A*, 2005, **109**, 8661.
20 H. Kawamata and K. Liu, *J. Chem. Phys.*, 2010, **133**, 124304.
21 J. Zhang, S. A. Lahankar, D. J. Garton, T. K. Minton, W. Zhang and X. Yang, *J. Phys. Chem. A*, 2011, **115**, 10894.
22 L. Schnieder, K. Seekamp-Rahn, E. Wrede and K. H. Welge, *J. Chem. Phys.*, 1997, **107**, 6175.
23 B. R. Strazisar, C. Lin and H. F. Davis, *Science*, 2000, **290**, 958.
24 C. Lin, M. F. Witinski and H. F. Davis, *J. Chem. Phys.*, 2003, **119**, 251.
25 X. Yang, *Phys. Chem. Chem. Phys.*, 2011, **13**, 8112.
26 J. J. Lin, D. W. Hwang, S. Harich, Y. T. Lee and X. Yang, *Rev. Sci. Instrum.*, 1998, **69**, 1642.
27 H. Richter and J. B. Howard, *Prog. Energy Combust. Sci.*, 2000, **26**, 565.
28 J. Park, G. J. Nam, I. V. Tokmakov and M. C. Lin, *J. Phys. Chem. A*, 2006, **110**, 8729.
29 F. Zhang, X. Gu, Y. Guo and R. I. Kaiser, *J. Phys. Chem. A*, 2008, **112**, 3284.
30 R. I. Kaiser, D. S. N. Parker, M. Goswami, F. Zhang, V. V. Kislov, A. M. Mebel, J. Aguilera-Iparraguirre and W. H. Green, *Phys. Chem. Chem. Phys.*, 2012, **14**, 720.
31 S. A. Lahankar, J. Zhang, S. Garashchuk, G. C. Schatz and T. K. Minton, *J. Phys. Chem. Lett.*, 2013, **4**, 1315.
32 G. Capozza, E. Segoloni, F. Leonori, G. G. Volpi and P. Casavecchia, *J. Chem. Phys.*, 2004, **120**, 4557.
33 B. Fu, Y.-C. Han, J. M. Bowman, L. Angelucci, N. Balucani, F. Leonori and P. Casavecchia, *Proc. Natl. Acad. Sci. U. S. A.*, 2012, **109**, 9733.
34 X. Yang, J. Lin, Y. T. Lee, D. A. Blank, A. G. Suits and A. Wodtke, *Rev. Sci. Instrum.*, 1997, **68**, 3317.
35 C. C. Wang, Y. T. Lee, J. J. Lin, J. Shu, Y.-Y. Lee and X. Yang, *J. Chem. Phys.*, 2002, **117**, 153.
36 N. Hemmi and A. G. Suits, *J. Chem. Phys.*, 1998, **109**, 5338.
37 S.-H. Lee, C.-H. Chin, W.-K. Chen, W.-J. Huang and C.-C. Hsieh, *Phys. Chem. Chem. Phys.*, 2011, **13**, 8515.
38 C.-H. Chin, W.-K. Chen, W.-J. Huang, Y.-C. Lin and S.-H. Lee, *J. Phys. Chem. A*, 2012, **116**, 7615.
39 H. F. Davis, J. Shu, D. S. Peterka and M. Ahmed, *J. Chem. Phys.*, 2004, **121**, 6254.
40 D. A. Blank, N. Hemmi, A. G. Suits and Y. T. Lee, *Chem. Phys.*, 1998, **231**, 261.
41 P. A. Willis, H. U. Stauffer, R. Z. Hinrichs and H. F. Davis, *Rev. Sci. Instrum.*, 1999, **70**, 2606.
42 M. Oana, Y. Nakatsuka, D. R. Albert and H. F. Davis, *J. Phys. Chem. A*, 2012, **116**, 5039.
43 R. Z. Hinrichs, J. J. Schroden and H. F. Davis, *J. Phys. Chem. A*, 2008, **112**, 3010.
44 J. J. Schroden and H. F. Davis, *J. Phys. Chem. A*, 2012, **116**, 3508.
45 C. Huang, W. Li, A. D. Estillore and A. G. Suits, *J. Chem. Phys.*, 2008, **129**, 074301.
46 A. D. Estillore, L. M. Visger-Kiefer, T. A. Ghani and A. G. Suits, *Phys. Chem. Chem. Phys.*, 2011, **13**, 8433.

47 A. D. Estillore, L. M. Visger-Kiefer and A. G. Suits, *Faraday Discuss.*, 2012, **157**, 181.
48 A. D. Estillore, L. M. Visger and A. G. Suits, *J. Chem. Phys.*, 2010, **132**, 164313.
49 S. Souma, T. Sato, T. Takahashi and P. Baltzer, *Rev. Sci. Instrum.*, 2007, **78**, 123104.
50 F. Mühlberger, J. Wieser, A. Morozov, A. Ulrich and R. Zimmermann, *Anal. Chem.*, 2005, **77**, 2218.
51 R. Flesch, M. C. Schürmann, M. Hunnekuhl, H. Meiss, J. Plenge and E. Rühl, *Rev. Sci. Instrum.*, 2000, **71**, 1319.
52 N. E. Sveum, S. J. Goncher and D. M. Neumark, *Phys. Chem. Chem. Phys.*, 2006, **8**, 592.
53 G. C. Bjorklund, *IEEE J. Quantum Electron.*, 1975, **QE–11**, 287.
54 R. Hilbig and R. Wallenstein, *Appl. Opt.*, 1982, **21**, 913.
55 J. P. Marangos, N. Shen, H. Ma, M. H. R. Hutchinson and J. P. Connerade, *J. Opt. Soc. Am. B*, 1990, **7**, 1254.
56 E. Cromwell, T. Trickl, Y. T. Lee and A. H. Kung, *Rev. Sci. Instrum.*, 1989, **60**, 2888.
57 S. J. Hanna, P. Campuzano-Jost, E. A. Simpson, D. B. Robb, I. Burak, M. W. Blades, J. W. Hepburn and A. K. Bertram, *Int. J. Mass Spectrom.*, 2009, **279**, 134.
58 M. Ahmed, D. S. Peterka and A. G. Suits, *Chem. Phys. Lett.*, 1999, **301**, 372.
59 R. Hilbig and R. Wallenstein, *IEEE J. Quantum Electron.*, 1983, **QE–19**, 1759.
60 R. Mahon and F. S. Tomkins, *IEEE J. Quantum Electron.*, 1982, **QE–18**, 913.
61 A. V. Smith and W. J. Alford, *J. Opt. Soc. Am. B*, 1987, **4**, 1765.
62 C. H. Muller, D. D. Lowenthal, M. A. DeFaccio and A. V. Smith, *Opt. Lett.*, 1988, **13**, 651.
63 M. Scheid, D. Kolbe, F. Markert, T. W. Hänsch and J. Walz, *Opt. Express*, 2009, **17**, 11274.
64 D. Proch and T. Trickl, *Rev. Sci. Instrum.*, 1988, **60**, 713.
65 D. L. Proctor, D. R. Albert and H. F. Davis, *Rev. Sci. Instrum.*, 2010, **81**, 023106.
66 P. A. Willis, H. U. Stauffer, R. Z. Hinrichs and H. F. Davis, *J. Phys. Chem. A*, 1999, **103**, 3706.
67 D. R. Albert, D. L. Proctor and H. F. Davis, *Rev. Sci. Instrum.*, 2013, **84**, 063104.
68 D. W. Kohn, H. Clauberg and P. Chen, *Rev. Sci. Instrum.*, 1992, **63**, 4003.
69 E. N. Sharp, M. A. Roberts and D. J. Nesbitt, *Phys. Chem. Chem. Phys.*, 2008, **10**, 6592.
70 V. Aristov, D. Conroy and H. Reisler, *Chem. Phys. Lett.*, 2000, **318**, 393.
71 J. M. Beames, F. Liu, M. I. Lester and C. Murray, *J. Chem. Phys.*, 2011, **134**, 241102.
72 R. Engleman, *J. Mol. Spectrosc.*, 1974, **49**, 106.
73 F. Leonori, K. M. Hickson, S. D. Le Picard, X. Wang, R. Petrucci, P. Foggi, N. Balucani and P. Casavecchia, *Mol. Phys.*, 2010, **108**, 1097.
74 P. Maksyutenko, D. S. N. Parker, F. Zhang and R. I. Kaiser, *Rev. Sci. Instrum.*, 2011, **82**, 083107.
75 J. Appel, H. Bockhorn and M. Frenklach, *Combust. Flame*, 2000, **121**, 122.
76 I. V. Tokmakov, G. S. Kim, V. V. Kislov, A. M. Mebel and M. C. Lin, *J. Phys. Chem. A*, 2005, **109**, 6114.
77 W. B. Miller, S. A. Safron and D. R. Herschbach, *Discuss. Faraday Soc.*, 1967, **44**, 108.
78 X. Gu, F. Zhang and R. I. Kaiser, *Chem. Phys. Lett.*, 2007, **448**, 7.
79 D. S. N. Parker, F. Zhang and R. I. Kaiser, *J. Phys. Chem. A*, 2011, **115**, 11515.
80 D. R. Albert and H. F. Davis, *J. Phys. Chem. Lett.*, 2010, **1**, 1107.
81 P. J. Linstrom and W. G. Mallard, *NIST Chemistry WebBook*, NIST, Gaithersburg, MD, 2005.
82 C.-Y. Lin and M. C. Lin, *Int. J. Chem. Kinet.*, 1985, **17**, 1025.
83 M.-F. Lin, Y. T. Lee, C.-K. Ni, S. Xu and M. C. Lin, *J. Chem. Phys.*, 2007, **126**, 064310.
84 C.-M. Tseng, Y. T. Lee, M.-F. Lin, C.-K. Ni, S.-Y. Liu, Y.-P. Lee, Z. F. Xu and M. C. Lin, *J. Phys. Chem. A*, 2007, **111**, 9463.
85 C.-M. Tseng, Y. T. Lee and C.-K. Ni, *J. Phys. Chem. A*, 2009, **113**, 3881.
86 D. R. Albert, M. A. Todt and H. F. Davis, *The Role of Collision Energy in the Phenyl + O_2 Reaction*, to be submitted.
87 X. Gu and R. I. Kaiser, *Acc. Chem. Res.*, 2009, **42**, 290.
88 D. Krajnovich, F. Huisken, Z. Zhang, Y. R. Shen and Y. T. Lee, *J. Chem. Phys.*, 1982, **77**, 5977.
89 R. E. Center and A. Mandl, *J. Chem. Phys.*, 1972, **57**, 4104.
90 B. Yang, J. Wang, T. A. Cool, N. Hansen, S. Skeen and D. L. Osborn, *Int. J. Mass Spectrom.*, 2012, **309**, 118.
91 Z. Zhou, M. Xie, Z. Wang and F. Qi, *Rapid Commun. Mass Spectrom.*, 2009, **23**, 3994.
92 J. D. Savee, S. Soorkia, O. Welz, T. M. Selby, C. A. Taatjes and D. L. Osborn, *J. Chem. Phys.*, 2012, **136**, 134307.
93 Z. Zhou, M. Xie, Z. Wang and F. Qi, *Rapid Commun. Mass Spectrom.*, 2009, **23**, 3994.
94 T. Adam and R. Zimmermann, *Anal. Bioanal. Chem.*, 2007, **389**, 1941.
95 J. C. Robinson, N. E. Sveum and D. M. Neumark, *J. Chem. Phys.*, 2003, **119**, 5311.
96 M. L. Morton, L. J. Butler, T. A. Stephenson and F. Qi, *J. Chem. Phys.*, 2002, **116**, 2763.
97 F. Aguirre and S. T. Pratt, *J. Chem. Phys.*, 2005, **122**, 234303.
98 H. Fan and S. T. Pratt, *J. Chem. Phys.*, 2006, **124**, 114312.
99 R. L. Gross, X. Liu and A. G. Suits, *Chem. Phys. Lett.*, 2002, **362**, 229.
100 W. R. Gentry, in *Atomic and Molecular Beam Methods*, ed. G. Scoles, Oxford University Press, New York, 1988, vol. 1, pp. 54–82.
101 J. J. Lin, *Phys. Chem. Chem. Phys.*, 2011, **13**, 19206.
102 P. C. Engelking, *Rev. Sci. Instrum.*, 1986, **57**, 2275.
103 J. A. Mueller, B. F. Parsons, L. J. Butler, F. Qi, O. Sorkhabi and A. G. Suits, *J. Chem. Phys.*, 2001, **114**, 4505.
104 W. Sun, K. Yokoyama, J. C. Robinson, A. G. Suits and D. M. Neumark, *J. Chem. Phys.*, 1999, **110**, 4363.
105 *NIST-JANAF Thermochemical Tables*, ed. J. Chase and W. Malcolm, American Chemical Society, Washington, DC, 1998.

106 S. Stolte, in *Atomic and Molecular Beam Methods*, ed. G. Scoles, Oxford University Press, New York, 1988, vol. 1, pp. 631–652.
107 S. R. Leone, M. Ahmed and K. R. Wilson, *Phys. Chem. Chem. Phys.*, 2010, **12**, 6564.
108 W. Sun. K. Yokoyama, J. C. Robinson, A. G. Suits and D. M. Neumark, *J. Chem. Phys.*, 1999, **110**, 4363.
109 O. Welz, J. D. Savee, D. L. Osborn, S. S. Vasu, C. J. Percival, D. E. Shallcross and C. A. Taatjes, *Science*, 2012, **335**, 204.
110 C. A. Taatjes, N. Hansen, D. L. Osborn, K. Kohse-Höinghaus, T. A. Cool and P. R. Westmoreland, *Phys. Chem. Chem. Phys.*, 2008, **10**, 20.
111 U. Even, J. Jortner, D. Noy, N. Lavie and C. Cossart-Magos, *J. Chem. Phys.*, 2000, **112**, 8068.
112 S. J. Greaves, R. A. Rose and A. J. Orr-Ewing, *Phys. Chem. Chem. Phys.*, 2010, **12**, 9129.
113 K. Honma and Y. Matsumoto, *Phys. Chem. Chem. Phys.*, 2011, **13**, 8236.
114 J. C. Weisshaar, *Acc. Chem. Res.*, 1993, **26**, 213.
115 M. A. Todt, D. R. Albert and H. F. Davis, High Intensity VUV and XUV Generation by Noncollinear Phasematching in Laser Vaporized Media, to be submitted.
116 S. Hannemann, U. Hollenstein, E.-J. van Duijn and W. Ubachs, *Opt. Lett.*, 2005, **30**, 1494.